PRECESSIONAL FLOW MACRO-INSTABILITIES IN STIRRED VESSELS: STUDY OF VARIATIONS IN TWO LOCATIONS THROUGH CONDITIONAL PHASE-AVERAGING AND CROSS-CORRELATION APPROACHES

M. Micheletti[1] and M. Yianneskis [1]

[1]Experimental and Computational Laboratory for the Analysis of Turbulence (ECLAT),

Department of Mechanical Engineering, King's College London, Strand, London,

WC2R 2LS, United Kingdom

michael.yianneskis@kcl.ac.uk

martina.micheletti@kcl.ac.uk

ABSTRACT

The precessional flow macro-instabilities were studied in a vessel stirred by a Rushton turbine with a multi-point laser-Doppler anemometry (LDA) system and flow visualization. The instability frequency, its variation with Reynolds number (Re) and its energy distribution throughout the vessel were investigated. Conditional sampling of the phase-resolved velocity data over a period of one vortex cycle showed a well defined cyclic variation of the mean velocity. 2-D velocity measurements, obtained simultaneously at two locations, indicated that the precessional vortex motion is well organised and that the precession axis, which defines the locus of the centre of the upper and lower vortices, is rotating in the same direction as the impeller but with a phase difference between the upper and lower parts of the tank.

1. INTRODUCTION

Mixing vessels are widely encountered in the chemical and pharmaceutical industries and are employed for a large number of operations. For this reason the single- and multi-phase flow fields have been studied extensively in a stirred tank in order to improve the efficiency of a particular mixing task. It is generally well known that turbulence plays a crucial role in the flow hydrodynamics and is widely responsible for the overall mixing performance in a vessel; recently, turbulence levels have been reported to be strongly affected by the presence of macro-instabilities (MIs) of the flow.

MIs are temporal mean flow variations that may change the flow pattern thus affecting the mixing efficiency. Bittorf and Kresta (2000) showed that the active volume of mean circulation in some cases is not the whole tank but has a height equal to 2/3 the tank diameter, although the upper volume is still involved in the overall mixing by macro-instabilities (Bruha et al., 1995). Multi-phase and reaction systems as well as heat transfer processes could also be strongly affected by the presence of such instabilities in the flow.

Different types of instabilities have been identified in the last two decades. One kind of instability has been observed to stem from changes in the off-bottom clearance, Nienow (1968) was among the first to observe that the flow pattern produced by a Rushton turbine could be either radial or axial depending on the value of the off-bottom clearance to vessel diameter ratio (C/T). Recently, Montante et al. (1999) showed that the mean flow transition from double to single-loop pattern, observed in a vessel stirred by a Rushton turbine, happens for values of C/T around 0.2. In vessels stirred by dual Rushton impellers different flow patterns are also present, depending on the separation between the two impellers and the clearance of the lower impeller from the vessel bottom (Rutherford et al., 1996). Changes in the circulation flow pattern produced by pitched blade turbines (PBTs) with C/T have also been reported; Kresta and Wood (1993) observed a significant change in the impeller discharge angle with a PBT when the clearance was increased from T/3 to T/2.

A second type of instability is associated with changes in Reynolds number (Re) or impeller speed (N). Nouri and Whitelaw (1990) and Hockey and Nouri (1996) reported that the flow pattern produced by a PBT changed from mainly radial to mainly axial flow at Reynolds numbers of 490 and 1200, respectively.

Another type of instability involves a forced vortex moving around the shaft axis with a certain frequency. Yianneskis et al. (1987) first observed this type of macro-instability of the mean flow, in a vessel stirred by a Rushton impeller set at C = T/3, which was moving with a frequency of around 0.02N. Haam. et al. (1992) reported a periodic variation of the heat transfer coefficient and attributed the oscillations to a precession of an axial vortex around the vessel.

Recently, a large number of studies have dealt with the latter instability. Bruha et al. (1995) used a "tornadometer" device to study the macro-instabilities (MI) phenomenon for a wide range of Re (4200-67000) in a vessel stirred by a 45º PBT (impeller diameter D = T/3, C = 0.35T); they reported a linear dependence of the MI frequency on the impeller speed, N, which is expressed by Equation (1):

$$f = aN\text{-}b \qquad (1)$$

Where a = 0.041-0.05 and b = 0.009-0.04. This work was extended to lower Re numbers in the same geometry vessel by Bruha et al. (1996), who reported no MI frequency present below Re = 200. For 200 < Re < 5000 the MI frequency was noted to increase with Re but no analytical expression was derived in this case. Finally, for Re > 9000 the ratio of the instability frequency, f, to the impeller rotational speed (N) was found to be almost constant. The dimensionless frequency, f', is expressed by Equation (2):

$$f' = \frac{f}{N} \qquad (2)$$

Bruha et al. (1996) reported a value of f' around 0.043-0.048. In a related work, Montes et al. (1997) studied the macro-instability phenomenon using laser Doppler velocimetry (LDV) and flow visualization; they concluded that a low-frequency non-stationary pseudo-periodic motion is present between the impeller plane and the free surface and its dominant frequency is linearly coupled with the impeller speed according to Equation (2), with f' being equal to 0.0575. Hasal and Fort (2000) carried

out a proper orthogonal decomposition (POD) and spectral analysis to extract the energy content of the macro-instability motion from the velocity data obtained at three different Reynolds numbers; the corresponding values of the dimensionless frequency were f' = 0.09 (Re = 750), f' = 0.0855 (Re = 1200) and f' = 0.0593 (Re = 75000).

Roussinova et al. (2000) measured the velocity time series for four impellers (PBT, A310, HE3 and RT) with LDV varying the impeller diameter, D, the number of baffles and the off-bottom clearance. They concluded that not only the MI frequency is sensitive to the geometry of the impeller, but it can also result in a broadening of the turbulent levels by up to 50%. Roussinova and Kresta; Roussinova et al. (2003) studied the spatial distribution of velocity macro-instabilities in a T = 0.24 m tank stirred by a 45º PBT and A310 impellers. In the case of the PBT with D = T/2 and C = T/2 a resonant frequency was identified, which remained dominant when the impeller was set at different clearances. Moreover, at Re > 10000, the MI frequency scaled with the rotational speed (f' = 0.18). The work was extended to a larger diameter vessel (T = 1.22 m) by Roussinova et al. (2003); the same dimensionless frequency, f' = 0.186, was obtained from experimental results and large eddy simulations (LES) predictions in both scales.

Myers et al. (1997) used Digital Particle Image Velocimetry (DPIV) to study the instability of the flow field produced by a 4 blades 45º PBT (D = 0.35T) and Chemineer HE-3 (D = 0.39T). The power spectral density (PSD) of the spatially-averaged vorticity data revealed the presence of a dominant frequency with periods around 42-88 seconds at an impeller speed N = 60 rpm, i.e. they obtained dimensionless frequency values of 0.011-0.02 at Re = 10500. Guillard et al. (2000) employed a laser induced fluorescence (LIF) technique to investigate the presence of large-scale coherent mixing structures which become unstable with an increase in impeller speed and that can be related to the vortex events observed near the surface and around the baffle by Yianneskis et al. (1987).

The mean flow and turbulence fields in a vessel stirred by a Rushton turbine and a pitched blade turbine have been investigated by Nikiforaki et al. (2003) with laser-Doppler anemometry (LDA) to characterise the macro-instabilities present in such flows. The frequency of the MIs was found to be linearly related to the rotational speed of the impeller and to be essentially independent of impeller design. A single fundamental frequency around 0.015-0.02N was present for all configurations; in addition, laser-sheet flow visualization experiments indicated clearly that the macro-instability stems from a precessional motion around the vessel axis similar to that encountered in most swirling flows. The dimensionless instability frequencies (f') determined in Nikiforaki et al.'s work are in agreement with the work of Winardi and Nagase (1991) with a marine propeller which yielded average lifetimes of unstable motions with f' = 0.02-0.03. Recently, PIV measurements carried out in a 100 mm tank stirred by a Rushton turbine (D = T/3, C = T/2) at Re = 40000 (Baldi, 2004) were also characterized by f' = 0.017. Hartmann et al. (2004) predicted the flow produced by a Rushton turbine (D = T/3, C = T/2) using LES and identified a whirlpool type of precessing vortex with a distinct frequency of 0.0255N and 0.0228N at Reynolds numbers of 20000 and 30000 respectively.

The aforementioned findings have shown that a macro-instability phenomenon is certainly present in stirred vessel flows. However the values of f' reported vary considerably (0.01-0.2). It is noteworthy that these investigations employed different measurement techniques, impeller types, tank sizes and operating conditions; in addition, logarithmic representation of the spectra and low sampling times and/or data rates might also affect the f' values reported (Nikiforaki et al., 2003).

To date there is still much uncertainty on the origin of such flow motions. The flow visualization study by Montes et al. (1997) showed the turbulent macro-instabilities as vortex structures present between the impeller and the liquid surface which modify the flow pattern in a regular, organised way. Based on the LES simulations results, Roussinova et al. (2003) identified three possible mechanisms that can drive MIs in the specific geometry studied (45º PBT, D = T/2, C = T/2): the impingement of the jet-like impeller discharge stream on the tank walls, the inward flow deflected from the baffles in a double-loop configuration at the tank bottom and the trailing vortex which combines with the re-circulation flow at the bottom of the tank to drive the upper circulation loop up along the tank. Finally, both the flow visualization carried out by Nikiforaki et al. (2003) and the computational fluid dynamics predictions (CFD) by Hartmann et al. (2004) clearly showed that MIs stems from a "whirlpool" vortex precessing around the shaft axis. However, in Nikiforaki et al.'s work the LDA velocity measurements were limited to locations close to the liquid surface, when a Rushton turbine was used, and it is not clear how the vortex motion propagates in the remainder of the vessel.

A recent investigation by Galletti et al. (2004) has shown that different types of instabilities, those present in a vessel at all times and for most configurations (Nikiforaki et al., 2003) and constantly or intermittently for specific configurations (Roussinova et al., 2003, Galletti et al., 2004) can be present simultaneously in a vessel and vary substantially in magnitude depending on the location.

Another issue that is not fully resolved is the nature and frequency of the MIs in non-turbulent flows. Montes et al. (1997) reported values of f' = 0.09 and f' = 0.0855 at Re = 750 and Re = 1200, respectively, in a vessel stirred by a PBT. Galletti et al. (2004) found out that the macro-instabilities stemming from precessional motions are characterised by two frequencies, one present at low Re and another at high Re; in both cases the MIs frequencies were linearly related to the impeller speed but had different values of the proportionality constant. However, the mechanism involved in the transition from the low to the high Re macro-instability and the characteristics of the two types of vortex motion are not fully understood.

This work investigates the macro-instabilities phenomenon in a vessel stirred by a Rushton turbine, set both at C = T/3 and C = T/2 clearances, in order to shed light into the characteristic frequency and origin of such motions by means of spectral analysis and flow visualization techniques, respectively, for a wide range of Reynolds numbers. A theoretical analysis of the flow field was also carried out to investigate the relation between the frequency of the precession and the tangential velocity magnitudes in regions close to the liquid surface. The velocity recordings were obtained with a multi-point LDA technique at several locations in the vessel in order to study the propagation of the vortex motion across the vessel and to characterise the shape of the precession axis.

The remainder of this paper is divided in three sections. First, the geometry of the stirred vessel and the flow conditions used in the experimental investigation are described, together with the main characteristics of the experimental techniques employed and the spectral analysis parameters. The results obtained are presented and discussed in section 3 for the two vessel geometries where the measurements were carried out and the paper closes with a list of concluding remarks.

2. STIRRED VESSEL CONFIGURATION AND EXPERIMENTAL TECHNIQUES

2.1 Vessel and impeller configurations

In the LDA measurements two vessels were employed, with internal diameters T = 80.5 and 294 mm, respectively. Both of them were standard configuration cylindrical mixing tank of height (H) equal to the tank diameter, T, equipped with four equally spaced vertical baffles of width B = T/10 and thickness $t_b \cong$ T/100. A six-bladed Rushton turbine of diameter D, with a blade width of 0.2D, was used. In all experiments the impeller was set at a clearance from the vessel bottom, C, equal to either T/3 or T/2. The dimensions of the mixing vessels and their impellers are listed in Table 1. A schematic representation of the stirred vessel and Rushton impeller configuration is shown in Figure 1 (a) and (b) along with the various measurement locations that will be described extensively later on in this work (Figure 1 (c), (d), (e)). In both cases the vessel was encased by a square trough in order to minimize refraction through the cylindrical surface and a lid was placed at a height H = T in order to prevent air entrainment at the highest speeds. Nikiforaki et al. (2003) have previously reported that the presence of the lid did not affect the macro-instability precessional motion around the vessel.

Table1. Dimensions of the vessels and the impellers employed (dimensions in mm).

Vessel	**1D LDA**	**2D LDA**
Diameter, T	80.5	294
Height, H	80.5	294
Baffle width, B	8.5	30
Baffle thickness, t_b	1	3
Impeller		
Diameter, D	27	98
Blade thickness, t	1	3

A cylindrical coordinate system is used, with the radial, axial and azimuthal coordinates indicated in the following text by r, z and θ, respectively. Its origin is positioned in the centre of the vessel bottom

and $\theta = 0^o$ (or 60^o) corresponded to a plane located half-way between two baffles. In this work U_i is the instantaneous velocity in the i^{th} direction, $\overline{U}_i$ is the mean velocity component and u_i' is the root mean square (r.m.s.) of the corresponding fluctuating velocity (with i being independently r, z or ?).

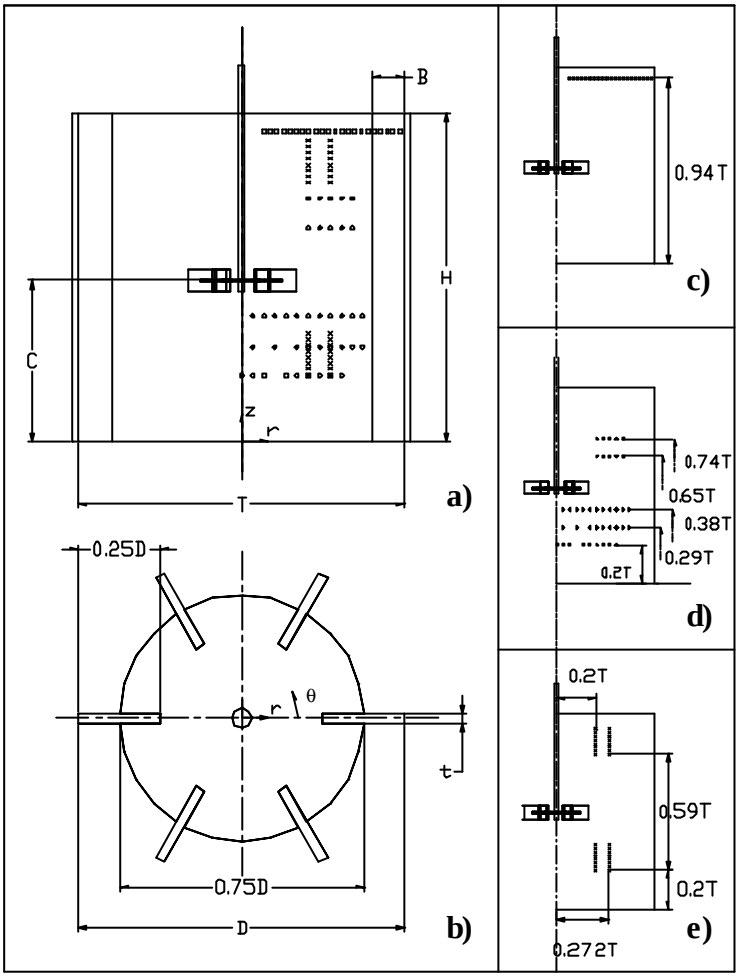

Figure 1. Geometry of the vessel and of the Rushton impeller and main measurement locations.

2.2 Experimental techniques

2.2.1 LDA Technique

A four-channel Dantec Ltd. LDA system mounted on a traverse that can be moved in three orthogonal directions was employed for the measurements; the main characteristics of the system have been described in detail by Micheletti (2004). Both 1-D and 2-D velocity measurements were carried out with different probes arrangement and measurement locations.

Firstly 1-D velocity measurements were obtained in the 80.5 mm vessel at z/T = 0.944 and at various radial locations (Figure 1 (c)). Both the transition and turbulent regimes were investigated (Re $\in$ [8500; 42500]). The probe was used with a lens of 240 mm focal length; the resulting control volume dimensions are 0.034 x 0.034 x 0.22 mm^3. In this case the probe axis was always perpendicular to the vessel axis. The fluid employed was a mixture of 41% tetraline, 28% 1-methylnaphtalene and 31% 1-chloronaphtalene by volume, with density ρ = 1050 kg/m^3 and a dynamic viscosity equal to one and a half times that of water. The refractive index of the mixture was measured using an Abbé refractometer (sodium D light) and it was found to be $\mu = 1.5903$ at 20^o.

A 2-D probe was employed to measure simultaneously the tangential and radial component of the velocity at various locations in the 294 mm vessel (Figure 1 (d)). The probe axis was set parallel to the vessel axis and optical access was obtained through the transparent bottom of the vessel. Moreover, simultaneous measurements of the radial velocity component at two locations were obtained by using a pair of beams of the 2-D probe and an additional 1-D probe forming an angle of 28º with the z-direction. The two probes were then moved along the vertical direction by keeping constant the distance, measured along the vertical direction, between the two measurement points (d = 0.64T). LDA velocity data were collected in 5 pairs of points, whose exact location was calculated using geometrical considerations and Snell's law of refraction (Equation (3)):

$$\frac{\sin(\alpha)}{\sin(\alpha')} = \frac{\mu'}{\mu} \qquad (3)$$

Where α and α' are the angles formed by the beam direction and the refracted beam direction, respectively, with the normal direction to the plane between the two media (π plane) and μ and μ' are the refractive indices of the two media. The measurement locations are shown schematically in Figure 1 (e). In all experiments carried out in the 294 mm vessel the working fluid was distilled water (μ = 1.33).

In all cases the light scattered was collected in backscatter mode and measurements were performed in a plane situated midway between two baffles (θ = 0º). The mixture was seeded with 10 μm silver-coated neutrally buoyant particles. Two burst spectrum analyzers were used to process the Doppler signals. Both 360º ensemble-averaged and angle-resolved (ensemble-averaged over 1º of impeller revolution) measurements were obtained. In the latter case it was noted that the data rate varied with angle; consequently, more than 500 samples per 1º interval of angle were collected, in order to have statistically independent values of mean velocity and turbulence level in each 1º window (Lee, 1995). At all locations a large number of data (varying from 200,000 to 500,000) were obtained to have results representative of the time scales of the flow motions studied. The impeller rotational speed, N, was measured with a shaft encoder and it was noted to vary by no more than ± 1%.

2.2.2 Spectral analysis

The velocity-time recordings were analysed using FFT techniques to obtain the energy distribution of the velocity fluctuations. Due to the fact that the samples collected using the LDA technique are unevenly distributed in time, the data were re-sampled using the "nearest neighbour" interpolation with a re-sampling frequency equal to half the mean measurement data rate. Frequency spectrum resolutions of the order of 0.001-0.01 Hz were used and in all cases the kinetic energy content of the velocity fluctuations, as obtained from the spectrum, was compared with that derived from the velocity measurements to confirm that the processing method did not affect the results.

2.2.3 Flow Visualization

Laser sheet flow visualization experiments were also carried out with an Argon laser (1.5 W) and a combination of lenses in the 294 mm vessel seeded with polystyrene particles (d_p = 800 μm). During these experiments the lid was removed in order to record the observations with a video camera. A horizontal light sheet was placed a few millimetres from the top surface to be able to visualize the flow in this area where the vortex motion is reported to be stronger. An aqueous sucrose solution with a sucrose content of 20% (N = 200 r.p.m., Re = 17600) and 40% (N = 100 r.p.m., Re = 2000) by weight was employed to be able to visualise the flow motion over a broader Re range.

3. RESULTS

3.1 Measurements in 80.5 mm vessel

Earlier investigations reported that the macro-instability phenomenon due to the vortex precessing motion was more pronounced and clearly defined in the region close to the liquid surface (Nikiforaki et al., 2003). This was confirmed by the flow visualization results obtained in this study, which showed the presence of a whirlpool-type vortex rotating around the vessel axis; an image extracted from the camera recordings is shown in Figure 2, where the arrows indicate the shaft rotation and the vortex

rotation directions. The vortex motion and that of the precession were in the same direction as the impeller rotation. Initially the region close to the top of the vessel was selected for more investigation. A characteristic radial component velocity-time trace over 4 seconds obtained with the Rushton turbine set at C = T/3 clearance is shown in Figure 3. The velocity recording, obtained at z/T = 0.944, r/T = 0.124 and at Re = 25500, shows a periodic variation of the mean velocity with a frequency (f) of 1.82 Hz corresponding to a period T = 0.56 seconds; additional higher frequency smaller amplitude non-turbulent fluctuations are present as well in the recording shown in Figure 3 as well as in most velocity-time recordings obtained throughout the vessel. The amplitude of the mean velocity variation is around 0.6 m/s, or $0.14V_{tip}$ ($V_{tip} = \pi ND$).

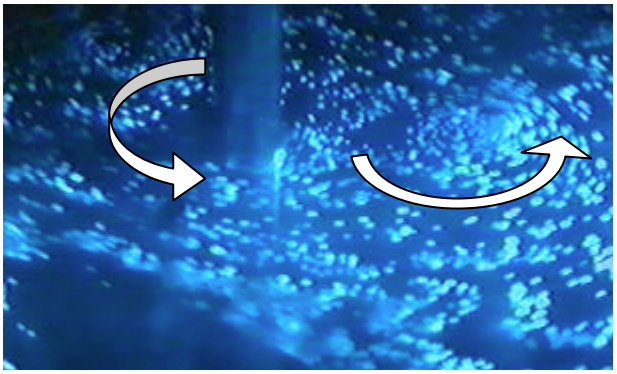

Figure 2. Image of the top of the vessel extracted from the flow visualization camera recordings; 294 mm vessel, C = T/2 (Re = 17600).

The velocity-time data were analysed using FFT to obtain the distribution of the kinetic energy of the turbulent fluctuations over various frequencies according to Equation (4) (Hinze, 1975):

$$\int_0^\infty E_i(f)\,df = u_i'^2 \qquad (4)$$

where E_i is the energy of the radial velocity component per unit of frequency and u_i' is the r.m.s. of the fluctuating velocity in the radial direction. The energy spectrum obtained from the velocity recordings of Figure 3 is shown in Figure 4. A well-defined peak is apparent at a frequency f = 1.82 Hz, while a second and a third harmonic are present at 3.9 Hz and 5.6 Hz, respectively. The ratio of the peak frequency over the rotational speed of the impeller (N = 3000 r.p.m.) was found to be f/N = 0.036.

LDA measurements conducted at lower Re showed again the presence of cyclic variation of the mean flow but with a higher f', superimposed on the turbulent fluctuations. Figure 5 shows the radial velocity-time trace obtained over 4 seconds at Re = 8500 (z/T = 0.944, r/T = 0.124). The amplitude of the mean velocity variation is around 0.2 m/s, or 0.14 V_{tip}, the same value obtained in the velocity recordings at high Re. However, the fluctuations have a frequency of 1.65 Hz (T = 0.6 s), which leads to f/N = 0.099. The energy spectrum obtained from these velocity recordings is plotted in Figure 6.

No other peaks were present in the energy spectra of the velocity recordings, obtained throughout the vessel in this study, at either the high or the low Re numbers. The energy associated with the MI peak depended significantly on the measurement location. Both the radial and tangential component velocity-time traces were analysed with FFT and resulted in the same MIs frequency as well as in the same energy distribution of the fluctuations over different frequencies. An extensive study of the MIs energy distribution in the vessel and a quantification of the influence of the macro-instabilities on the magnitude of the turbulence levels is presented later in this paper.

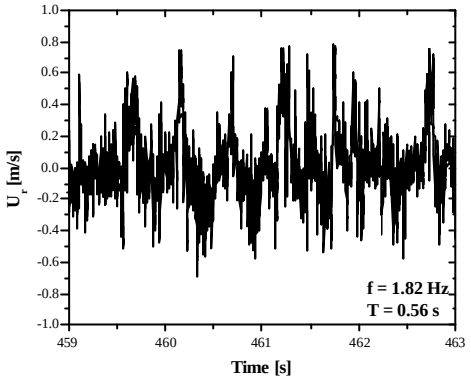

Figure 3. Radial instantaneous velocity variation with time at r/T = 0.124 and at z/T = 0.944; 80.5 mm vessel, C = T/3, N = 3000 rpm (Re = 25500).

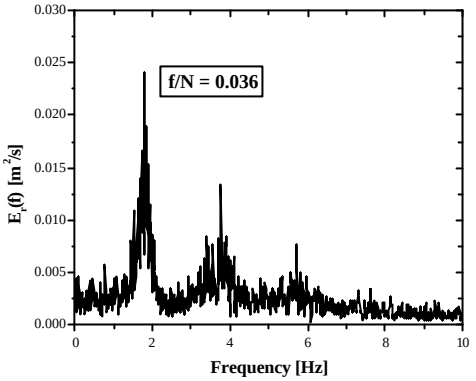

Figure 4. Energy spectra obtained from the radial velocity component measured at r/T = 0.124 and at z/T = 0.944, C = T/3, N = 3000 rpm (Re = 25500).

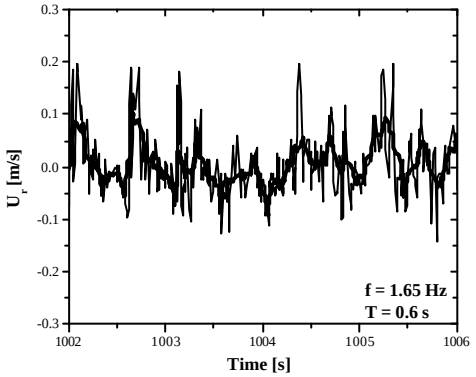

Figure 5. Radial instantaneous velocity variation with time at r/T = 0.124 and at z/T = 0.944, C = T/2, N = 1000 rpm (Re = 8500).

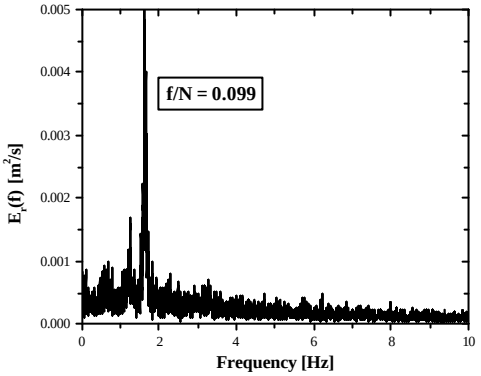

Figure 6. Energy spectra obtained from the radial velocity component measured at r/T = 0.124 and at z/T = 0.944, C = T/2, N = 1000 rpm (Re = 8500).

Both frequencies observed at high and low Re showed a linear variation with the impeller rotational speed but with a different proportionality constant. The variation of the characteristic MIs frequency with impeller rotational speed is shown in Figure 7 for the two geometric configurations in the range of Re studied together with the best linear fit. The slopes of the two straight lines, or the f/N ratios, for the low and high frequency instabilities are 0.03 and 0.08, respectively. When the Rushton turbine was set at C = T/3, the velocity measurements were carried out for Reynolds numbers in the range 4250-42500 ($N \in [8.3, 83.3\ s^{-1}]$); however, at Re < 17000 ($N < 33.3\ s^{-1}$) the spectral analysis did not show clearly the high frequency peak previously observed at low values of Re. On the other hand, measurements conducted with the Rushton turbine set at C = T/2 showed a single high frequency peak present at $Re \leq 8500$ ($N \leq 16.6\ s^{-1}$) while in the range $Re \in [8500\text{-}17000]$ both peaks were present in the same energy spectrum.

The energy spectra obtained in the transition range of Re, at which both peaks were present, with the Rushton turbine set at C = T/2 are presented in Figure 8. As has already been mentioned, at Re = 8500 only one high frequency peak is present in the energy spectrum, corresponding to values of f/N = 0.09-0.1, whose energy decreases with increasing Re until it decays totally at Re = 21200; a low frequency peak (f/N = 0.02) is poorly defined in the spectrum obtained at Re = 12750 but the energy associated with it increases for higher values of Re until it becomes the only instability present at Re > 20000. As it can be noted from Figure 8, an additional peak is also present at f/N approximately equal to 0.07. This is probably due to the phenomenon of "beating" caused by the superimposition of two sine waves

with frequencies f_1 and f_2; the "beat" frequency is the difference between the original frequencies, as expressed by Equation (5):

$$f_{beat} = |f_1 - f_2| \tag{5}$$

This observation made was confirmed by the fact that the intermediate peak, corresponding to f/N = 0.07, is present solely when *both* the other two frequencies are present in the energy spectrum.

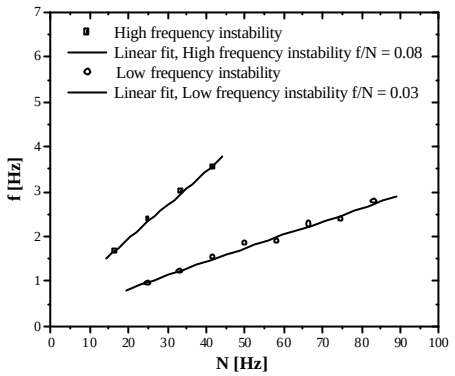

Figure 7. Frequency variation with impeller rotational speed at r/T = 0.124 and at z/T = 0.944.

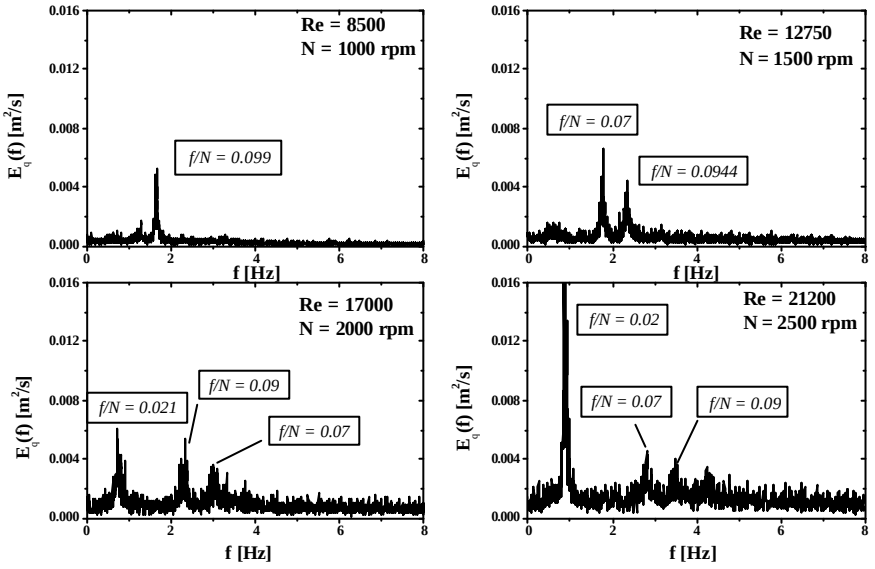

Figure 8. Energy spectra obtained from the tangential velocity component measured at r/T = 0.124 and at z/T = 0.944, C = T/2, N = 1000, 1500, 2000 and 2500 rpm.

The considerations made above suggest that there is a limited range of impeller speeds, or Reynolds numbers, in which the switch between the two characteristic frequencies takes place. Therefore, an attempt was made to improve the understanding of the transition mechanism from low to high Re through the assessment of the amount of energy involved in the two types of instability motions. The one-dimensional energy spectrum, $E_\theta(f)$, obtained using the tangential component velocity-time data was employed for this purpose; the energy associated with the instability peak can be calculated as the area under the peak and it was normalised with the total energy calculated from the spectrum at the specific location. The variation of the energy associated with the low frequency peak, $E_\theta(f_L)$, when this was the only one present in the energy spectrum, is plotted in Figure 9 (a) as a function of the radial location. At all Re investigated the low frequency MI is stronger in regions close to the vessel axis, where it contributes with more than 20% to the total energy content. No significant change of the energy radial profile with Re was noted in this specific case.

The radial profile of the energy associated with the high frequency peak, $E_\theta(f_H)$, is plotted in Figure 9 (b) for four different Re. It is noteworthy that only the high frequency peak was present in the energy spectra obtained at Re = 8500 and Re = 12750 while in the other two cases both peaks were observed. Two important observations are suggested by the curves plotted in Figure 9 (b): not only the shape of the energy distribution along the vessel radius is different from the one observed in the case of the low frequency MI, but the profiles appear to be affected by the flow Reynolds number. In all cases the energy distribution reaches a maximum which is approximately centred in r/T = 0.225; this implies that the high frequency vortex, although present at all radial locations, is stronger in the region 0.2 < r/T < 0.3. The maximum is achieved at the lowest Re investigated, Re = 8500, where the amount of energy associated with the high frequency instability is more then 20% of the total energy of the velocity fluctuations. As it can be noted from Figure 9 (b) the amount of energy decreases to approximately 12% at Re = 21200, when the low frequency peak is also present in the energy spectrum. Therefore it was considered instructive to ascertain how the energy is distributed between the two distinct phenomena in the transition range of Reynolds numbers.

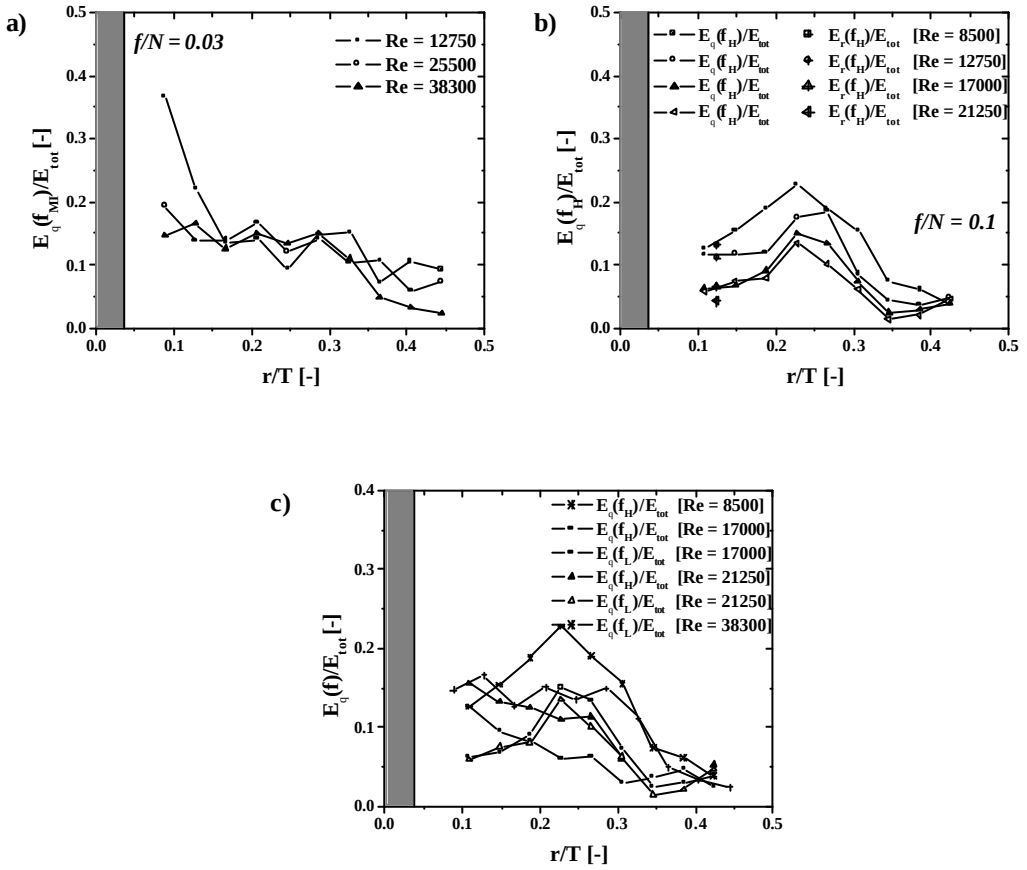

Figure 9. Normalized energy content of the MI motion at different Re numbers at z/T = 0.944: (a) Low frequency instability; (b) High frequency instability; (c) Low and high frequency instabilities.

Figure 9 (c) shows the energy profiles associated with each peak at two Re, along with the results obtained at Re = 8500 and at Re = 38000 where only one frequency was observed. At Re = 8500 the high frequency macro-instability is associated with the maximum amount of energy observed in this work; this energy decreases by almost half when Re is increased to 17000 and the low frequency vortex is also present, characterized by its own profile. When Re is further increased to 21200 the energy of the high frequency MI decreases while that associated with the low frequency one increases. To conclude, the energy involved in the two types of motion is at its maximum when only one frequency is present; this can be observed for both the low and high frequency MIs cases represented in Figure 9 (c) while at Re corresponding to the switch between the two instabilities the energy is divided into the two motions each maintaining, however, the characteristic shape of the radial profile.

Flow visualization results were carried out at different Reynolds numbers to be able to observe both the low and the high frequency phenomena when the Rushton impeller was set at C = T/2. At Re = 17600 (high Re number region) only one big vortex was observed to rotate relatively slowly around the shaft and it was lasting a few seconds. On the other hand the recordings obtained at a lower Re (Re = 2000) often revealed the presence of two vortices moving around the vessel axis at the same time. In addition, in the latter case the precession was faster, with the two vortices decaying near the shaft; the vortex centre location in both cases could not be determined with sufficient accuracy and the difference found between the two frequencies could not be explained by the flow visualization results only. It should be added that Czarny et al. (2002) conducted a visualization study of the flow produced between a stationary and a rotating disk. They reported that large-scale vortex structures may exist in axisymmetric geometries and, besides, they observed the tendency for the number of vortices to decrease as the Reynolds number is increased. Grosjean et al. (1997) also identified a precessing vortex core in a rotating cylinder flow caused by the fact that the flow rotation is not always centred in the geometric centre of the cylinder.

The presence of a big vortex, precessing around the shaft with a frequency f = 0.0255N at Re = 30000, was shown by the Large Eddy Simulation (LES) of Hartmann et al. (2004) in a vessel stirred by a Rushton turbine. Moreover, the snapshots of the flow field presented by Hartmann et al. (2004) at different locations also confirmed that the low frequency instability was observed to be more pronounced, in its strength and size, in a confined region close to the shaft at r/T < 0.1.

The results presented suggest that the frequency of the precession around the vessel axis may be related to the tangential velocity of the flow in the vicinity of the surface. The mean and r.m.s velocities were therefore measured along the radius for a range of Re, or impeller speeds, and are presented in Figures 10 and 11 for the C = T/3 and the C = T/2 clearances, respectively. The results are not normalised values to show a characteristic feature observed in this work. As can be noted from both Figures 10 (a) and 11 (a), all the mean velocity profiles in the tangential direction cross in one point at around r/T = 0.26; this essentially indicates that in this particular location the velocity, in absolute terms, remains constant as the impeller speed is increased. Correspondently, the r.m.s. velocity in the same direction presents a maximum, even though not very pronounced, at approximately the same radial location (Figure 10 (b) and 11 (b)). It is noteworthy that the all the velocity measurements in this work were carried out in a plane midway between two baffles (θ = 0º). Therefore, the fluid rotation motion around the vessel is influenced by the counter current re-circulation coming from the up stream baffle which is responsible for the negative mean velocity values at r/T values higher than 0.3. When the impeller speed is increased the fluid velocity increases, in absolute terms, both in regions close to the shaft and in the vicinity of the wall maintaining constant, however, the location of the inflection point which separates the part of the profile that arches upwards from the one arching downwards. It is interesting to note that this finding was only observed at z/T = 0.944 and not at the other locations where velocity measurements were taken (results not shown here for brevity). This may indicate the characteristics of this area of the vessel where the flow appears to be more akin to a free vortex, even though still influenced by the impeller rotation (i.e. through the linear relationship between MI frequency and impeller rotational speed).

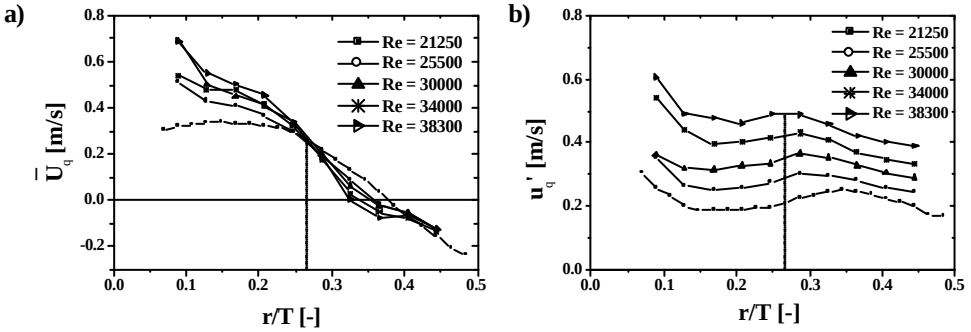

Figure 10. Radial profile of the tangential velocity at different Re and C = T/3: (a) mean velocity; (b) r.m.s. velocity.

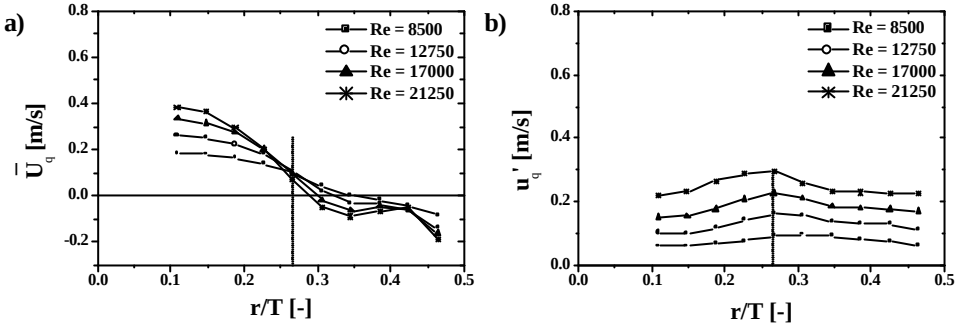

Figure 11. Radial profile of the tangential velocity at different Re and C = T/2: (a) mean velocity; (b) r.m.s. velocity.

Due to the characteristic shape of the tangential mean and r.ms. velocity profiles an effort was made to relate them to the vortex precession motion revealed by both the flow visualization results and the spectral analysis of the velocity-time recordings. For this purpose, a brief account of swirl flows and their characterization was considered necessary in order to thoroughly understand the instability behaviour. Swirl flows can be generated by direct rotation of a device, such as an impeller rotating in a cylindrical vessel. Rotating flows often have a central core of solid body rotation type, or forced vortex, characterized by a tangential velocity distribution as in Equation (6):

$$w_{rot} = c'r \tag{6}$$

Outside the central region, free (or potential) vortex conditions may prevail as are found in the atmosphere in whirlwinds, tornadoes, cyclones (Gupta et al., 1984). In such rotating flows the mean tangential velocity should decrease along the radius according to the following Equation (7):

$$w_{irrot} = \frac{C}{r} \tag{7}$$

The value of the constant C strongly depends on the type of flow and the geometric configuration; if the angular velocity of the shaft at the shaft radius r_o, $w_{ro} = 2\pi r_o N$, is equalized with the velocity of the surrounding fluid at the same radius, as calculated using Equation (7), a value of C = 0.0028 is obtained at N = 3000 rpm. A velocity distribution typical of free vortex flows with this value of C was then subtracted from the experimental mean tangential velocity profile and the results are shown in Figure 12 for Re = 25500. The velocity-curve obtained reveals a velocity distribution, approximately centred in r/T = 0.125, which is characteristic of a solid body rotation flow or forced vortex as described by Equation (6). The constant c' represents the frequency of the vortex rotation around its centre and it was equal to 0.6N for the data set presented in Figure 12. All the profiles analysed resulted in the same velocity distribution and in vortex frequencies around 0.4-0.7N. This finding is in close agreement with the axial vorticity results predicted at z/T = 0.12 and z/T = 0.88 by Hartmann et al. (2004) for a geometrically similar system at Re = 30000. Due to the stochastic nature of the instability phenomenon the above analysis represents only an attempt to link the measured velocity profiles and the MI on the vessel surface and it is meant to be only an approximated simplification of such complex 3-D motions present in a stirred vessel.

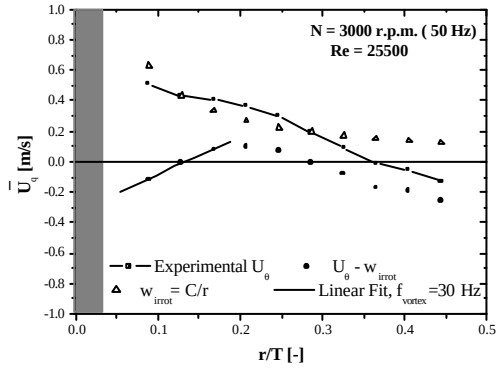

Figure 12. Tangential velocity variation with r/T at N = 3000 rpm (Re = 25500), C = T/3.

3.2 Measurements in the 294 mm vessel

2-D LDA measurements were carried out in a 294 mm vessel at different axial and radial locations to provide better understanding of the nature of the low frequency macro-instability motion and its propagation around the vessel. In this case the Rushton turbine was always set at a clearance C = T/2 and only one Reynolds number, Re = 27000, was studied.

The radial component velocity-time traces were analysed using FFT techniques and the energy distribution of the MI motion throughout the vessel was quantified from the energy spectra obtained. Figure 13 shows the normalised energy contour plot for a vertical plane located midway between two baffles (θ = 0º). A large area characterized by relatively low values of $E_r(f_L)/E_{tot}$ appears, located approximately in the centre of the plane and extending from z/T = 0.2 to z/T = 0.8. Although measurements in the region above the impeller were restricted by difficult optical access, it is clear from Figure 13 that MIs progressively increase in strength when moving from the aforementioned central zone to the top and bottom of the vessel at r/T < 0.2. The latter finding is in agreement with the energy profile obtained from the tangential velocity measurements in the 80.5 mm vessel at z/T = 0.944 (Figure 9 (a)). In particular, the area located below the impeller at z/T = 0.2 and r/T = 0 seems to be subjected to strong MI motions which contributed more than 40% to the total energy content.

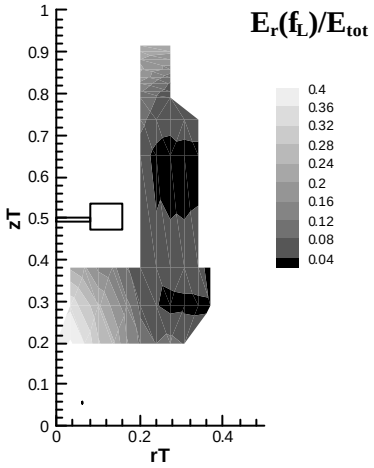

Figure 13. Contour plot of the normalised energy content of the MI as obtained from the radial velocity-time traces at different locations, 294 mm vessel, C = T/2, Re = 27000.

The f' value found from the data obtained in the 294 mm vessel was around 0.015-0.02; correspondingly, the number of impeller revolutions for the MI vortex to complete one cycle around the vessel axis was between 50 and 66. Conditional sampling of the phase-resolved data over a period of one vortex cycle around the vessel were made for the radial and tangential velocity components measured simultaneously. The results obtained are presented in Figure 14 for two different locations and show the cyclic variation of the mean velocity values over a period of approximately 60 impeller revolutions. Similar trends were observed, for both the radial and tangential velocity components, at all the locations where the measurements were made, being more pronounced in some cases due to the probabilistic nature of the MI phenomenon.

LDA measurements of the radial velocity component were carried out simultaneously at two locations, at z/T = 0.2 and z/T = 0.84, at r/T = 0.204, in order to analyse the relation between the velocity-time traces recorded in regions above and below the impeller, respectively. The normalised radial velocity-time traces obtained in the two locations are presented in Figures 15 (a) and (b); the low frequency content was also analysed using a moving-window averaging technique to filter out the turbulent high frequency fluctuations and the results are also shown in Figures 15 (a) and (b). A mean flow periodic variation corresponding to a period of approximately 20 seconds (f/N = 0.017) is apparent from both velocity-time traces. In addition, a phase difference is clearly present between the measurements obtained above and below the impeller.

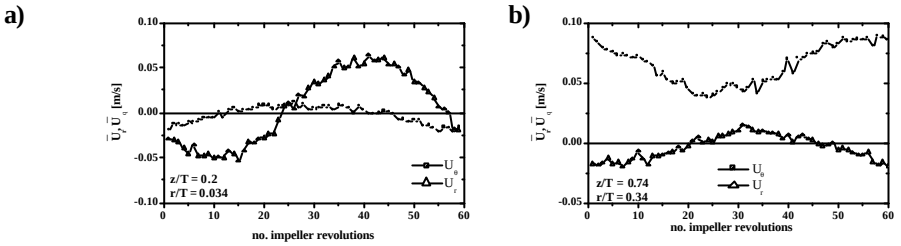

Figure 14. Angle-resolved radial and tangential velocity variation with number of impeller revolutions: (a) r/T = 0.034, z/T = 0.2; (b) r/T = 0.34, z/T = 0.74.

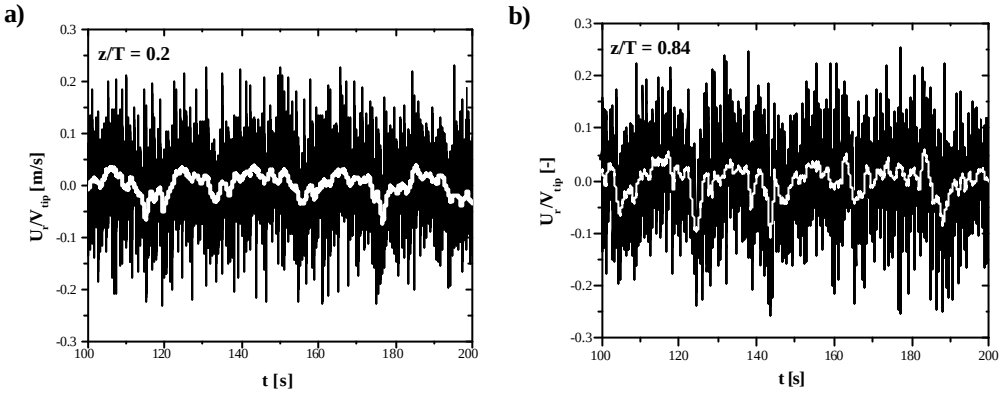

Figure 15. Normalised radial velocity-time trace at r/T = 0.204: (a) z/T = 0.2; (b) z/T = 0.84.

Due to the observed phase difference between the MI precession motions present in different regions of the vessel, 2-D measurements of the radial velocity component were also carried out for additional pairs of locations at r/T = 0.204 and r/T = 0.272 as described in section 2. The cross correlation index between the velocity-time series of each pair, $U_{r1}(t)$ and $U_{r2}(t)$, was calculated in order to quantify the angle difference between them according to Equation (8):

$$R(j) = \frac{\overline{u_{r1}(t)\,u_{r2}(t + j\cdot\tau)}}{u'_{r1}(t)\,u'_{r2}(t + j\cdot\tau)} \qquad (8)$$

where τ is the time coincidence window and j is an integer ranging from 0 to 360; τ was set equal to 0.055 seconds, which corresponds to 1/360 of the time necessary for the vortex to complete one revolution around the vessel. The cross correlation index variation with the angle between the velocity-time curves is shown in Figure 16 for the results obtained at r/T = 0.204. In all cases the maximum of the curves corresponds to an angle of 182 degrees, which represents the phase difference between the instantaneous velocity-time series recorded above and below the impeller. This indicates that the vortex-type instability is moving around the vessel axis with a phase shift of 180º between the two regions. No phase difference was found among measurements at different elevations.

The 2-D measurements obtained at a larger radius showed that the value of the phase difference at the different locations was not constant. The cross correlation index obtained at r/T = 0.272 is presented in Figure 17 at Re = 27000. The maximum for the pair z/T = 0.2-0.84 corresponds to an angle of 165º, which increases to 195º for the pair z/T = 0.236-0.87. For the last two pairs of measurement locations, z/T = 0.254-0.893 and z/T = 0.308-0.947, it was more difficult to define an angle corresponding to the maximum value of the cross correlation index due to the smooth variation of the profile; however, an angle of around 210º can be observed in both cases. At a larger radius, therefore, the phase shift between the motions above and below the impeller was found to increase with z/T maintaining constant, however, the distance between the measurement heights. Having observed the distribution of the amount of energy associated with the instability it is possible that an organised precession motion is present with a phase shift, especially in regions close to the shaft. At higher values of r/T the MI becomes weaker and this may result in a less structured motion or in a less defined precession axis. On the other hand, a variation of the phase angle with r/T could be expected due to the fact that the vortex has to travel different paths around the vessel at different radii.

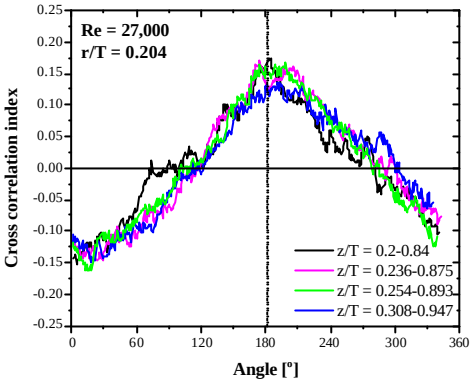

Figure 16. Cross correlation index variation with angle for various pairs of measurement heights, r/T = 0.204.

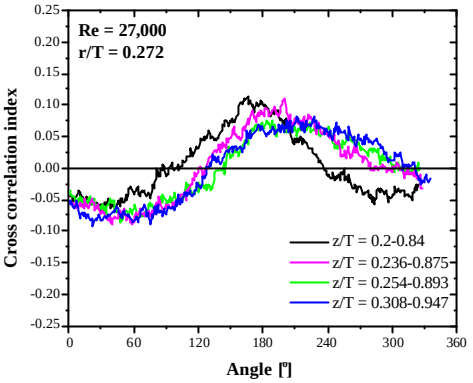

Figure 17. Cross correlation index variation with angle for various pairs of measurement heights, r/T = 0.272.

4. CONCLUDING REMARKS

The experimental investigation presented in this paper has shown some characteristic features of the macro-instability phenomenon and has provided novel information on its propagation around a stirred vessel. The instability frequency and its variation with Re along with its energy distribution throughout the vessel were investigated for two geometrical configurations with a multi-point LDA.

At high Re a single dominant peak was apparent from all the spectra obtained at different locations in the vessel. In the 294 mm vessel the value of f/N was found to be constant and equal to 0.015-0.2, as it was previously reported by Nikiforaki et al. (2003). Similar but slightly higher values (f/N = 0.03) were obtained from the measurements performed in the 80.5 mm vessel. The energy content associated with the MI was also found to contribute up to 40% to the total energy content of the spectrum and, consequently, MIs can be responsible for a significant broadening of the turbulence levels. Two regions, one close to the shaft in the top surface and the other below the impeller at z/T = 0.2, were characterized by the highest amount of MI energy.

At Re < 20000 a mean flow periodic variation was also observed, characterized by frequencies f/N = 0.09-0.1. Over a specific range of Re both frequencies were present and the transition region between the two motions was thoroughly investigated by evaluating the energy distribution and flow visualization.

The flow field in the top of the vessel, where the MIs were found to be stronger, was also studied; a velocity distribution typical of a forced vortex was obtained, with frequencies of the order of the impeller rotational speed. Although simplified, this analysis offered new information on the precession motion and on the characteristics of the vortex velocity distribution.

The results obtained also indicated that the precessional vortex motion is well organised throughout the vessel, with the precession axis, which defines the locus of the centres of the upper and lower vortices, rotating in the same direction as the impeller but with a 180º difference between the upper and lower parts of the tank.

The data offers useful and novel insights into the MI flow structures as well as the means for their characterisation. However, due to the complexity of the 3-D flow field present in a stirred vessel some questions still remain. The characterisation of the precession axis, for example, and especially its variation with radial location could be further extended; detailed 2-D velocity measurements could be carried out simultaneously at two or three locations by varying the axial and radial distance between them. In addition, such investigation could be interesting in other vessel/impeller configurations. New information was also provided in the Re transition region, where both high and low frequency instabilities are present; however, the origin of such transition is still not clear and further study is necessary in order to fully understand the MI behaviour.

REFERENCES

Baldi, S. (2004). "Energy dissipation measurements in stirred vessels with particle image velocimetry", Ph.D. Thesis, King's College London, London, UK.

Bittorf, K.J. and Kresta, S.M. (2000). "Active volume of mean circulation for stirred tanks agitated with axial impellers", *Chemical Engineering Science*, 55, pp. 1325-1335.

Bruha, O., Fort, I. and Smolka, P. (1995). "Phenomenon of turbulent macro-instabilities in agitated systems", *Collect.Czech.Chem.Commun.*, 60, pp. 85-95.

Bruha, O., Fort, I., Smolka, P. and Jahoda, M. (1996). "Experimental study of turbulent macroinstabilities in an agitated system with axial high-speed impeller and with radial baffles", *Collect.Czech.Chem.Commun.*, 61, pp. 856-867.

Czarny O., Iacovides, H. and Launder, B.E. (2002). "Precessing vortex structures in turbulent flow whithin rotor-stator disc cavities", *Flow, turbulence and combustion*, 69, pp. 51-61.

Galletti, C., Brunazzi, E., Yianneskis, M. and Paglianti, A. (2003). "Spectral and wavelet analysis of the flow pattern transition with impeller clearance variations in a stirred vessel", *Chemical Engineering Science*, 58, pp. 3859-3875.

Galletti, C., Lee, K.C., Paglianti, A. and Yianneskis, M. (2004). "Reynolds number and impeller diameter effects on instabilities in stirred vessels", *AIChE Journal* (In press).

Galletti, C., Paglianti, A. and Yianneskis, M. (2004). "Observations on the significance of instabilities, turbulence and intermittent motions on fluid mixing processes in stirred reactors", Proc. ISMIP-5 conference, Seville, June 2004.

Grosjean, N., Graftieaux, L., Michard, M., Hubner, W., Tropea, C. and Volkert, J. (1997). "Combining LDA and PIV for turbulence measurements in unstedy swirling flows", *Measurement science technology*, 8, pp. 1523-1532.

Guillard, F., Tragardh, C. and Fuchs, L. (2000). "A study on the instability of coherent mixing structures in a continuously stirred tank", *Chemical Engineering Science*, 55, pp. 5657-5670.

Gupta, A.K., Lilley, D.G. and Syred, N. (1984). Swirl flows, ABACUS Press.

Haam., S., Brodkey, R.S. and Fasano, J.B. (1992). "Local heat transfer in a mixing vessel using heat flux sensors", *Industrial and Engineering Chemistry Research*, 31, pp. 1384-1391.

Hartmann, H., Derksen, J.J. and van den Akker, E.A. (2004). "Macro-instability uncovered in a Rushton turbine stirred tank by means of LES", *AIChE Journal*, (In press).

Hasal, P.F.I. (2000). "Macro-instabilities of the flow pattern in a stirred vessel: detection and characterization using local velocity data", *Acta Polytechnica*, 40, pp. 55-67.

Hinze, J.O. (1972). Turbulence, Mc Graw Hill, 2nd Edition.

Hockey, R. and Nouri, J.M. (1996). "Turbulent flow in a baffled vessel stirred by a 60 pitched blade turbine", *Chemical Engineering Science*, 19, pp. 4405-4421.

Kresta, S.M. and Wood, P.E. (1993). "The mean flow pattern produced by a 45 pitched blade turbine: Changes in the circulation pattern due to off-bottom clearance", *Canadian Journal of Chemical Engineering*, 71, pp. 42-53.

Lee, K.C. (1995) "An experimental investigation of the trailing vortex structure and mixing characteristics of stirred vessels", Ph.D. Thesis, King's College London, London, UK.

Micheletti, M. (2004). "Study of fluid velocity and mixing characteristics in stirred solid-liquid suspensions", Ph.D. Thesis, King's College London, London, UK.

Montante, G., Lee, K.C., Brucato, A. and Yianneskis, M. (1999). "An experimental study of double-to-single-loop transition in stirred vessels", *The Canadian Journal of Chemical Engineering*, 77, pp. 649-659.

Montes, J.L., Boisson, H.C., Fort, I. and Jahoda, M. (1997). "Velocity field macro-instabilities in an axially agitated mixing vessel", *Chemical Engineering Journal*, 67, pp. 139-145.

Myers, K.J., Ward, R.W. and Bakker, A. (1997). "A digital Particle Image Velocimetry investigation of flow field instabilities of axial-flow impellers", *Journal of fluids engineering*, 119, pp. 623-632.

Nienow, A.W. (1968). "Suspension of solid particles in turbine agitated baffled vessels", *Chemical Engineering Science*, 23, pp. 1453-1459.

Nikiforaki, L., Montante, G., Lee, K.C. and Yianneskis, M. (2003). "On the origin, frequency and magnitude if macro-instabilities of the flows in stirred vessels", *Chemical Engineering Science*, 58, pp. 2937-2949.

Nouri, J.M. and Whitelaw, J.H. (1990). "Flow characteristics of stirred reactors with Newtonian and non-Newtonian fluids", *AIChE Journal*, 36, pp. 627-629.

Roussinova, V. and Kresta, S.M. (2000). "Analysis of macro-instabilities (MI) of the flow field in a stirred tank agitated with axial impellers", Proc. of the 10th Eur. Conf. on Mixing, Delft, The Netherlands.

Roussinova, V.T., Grgic, B. and Kresta, S.M. (2000). "Study of macro-instabilities in stirred tanks using a velocity decomposition technique", *Trans IChemE*, 78(Part A), pp. 1040-1052.

Roussinova, V.T., Kresta, S.M. and Weetman, R. (2003). "Low frequency macroinstabilities in a stirred tank: scale-up and prediction based on large eddy simulations", *Chemical Engineering Science*, 58, pp. 2297-2311.

Rutherford, K., Mahmoudi, S.M.S., Lee, K.C. and Yianneskis, M. (1996). "Hydrodynamic characteristics of dual Rushton turbine impeller stirred vessels", *American Institute of Chemical Engineers Journal*, 42, pp. 332-346.

Winardi, S. and Nagase, Y. (1991). "Unstable phenomena of flow in a mixing vessel with a marine propeller", *Journal of chemical Engineering of Japan*, 24 (2), pp. 243-249.

Yianneskis, M., Popiolek, Z. and Whitelaw, J.H. (1987). "An experimental study of the steady and unsteady flow characteristics of stirred reactors", *Journal of Fluid Mechanics*, 175, pp. 537-555.